Natural Hazards (2025) 121:2155–2192
https://doi.org/10.1007/s11069-024-06890-w

ORIGINAL PAPER

The aftermath of 2023 Kahramanmaras earthquakes: evaluation of strong motion data, geotechnical, building, and infrastructure issues

Selcuk Toprak[1] · A. Can Zulfikar[1] · Ahu Mutlu[1] · Ulgen Mert Tugsal[1] · Engin Nacaroglu[2] · Savas Karabulut[1] · Muhammet Ceylan[3] · Kamer Ozdemir[1] · Sedat Parlak[1] · Oguz Dal[1] · Sadra Karimzadeh[4]

Received: 15 July 2023 / Accepted: 17 August 2024 / Published online: 2 September 2024

Abstract
This paper presents the findings of field observations conducted in the aftermath of the earthquakes that struck the Pazarcik (Mw7.7) and Elbistan (Mw7.6) in Kahramanmaras province, Turkey on February 6th, 2023. The earthquakes, occurring on the East Anatolian Fault Zone (EAFZ), resulted in more than 50,000 losses of life and damage of more than 1.5 million properties across 11 provinces in Turkey. Field observations presented herein encompass seismological and strong ground motion data, geotechnical observations, as well as damage assessments of underground and above ground structures in various provinces and districts. The types and reasons of the structural damages were discussed. The study also examined the effects of high acceleration values and distribution of strong ground motions on the performance of structures. Soil liquefaction problems were observed in many locations such as Golbasi and Iskenderun. The paper highlights the geology, tectonics, strong motion characteristics, surface deformations, geotechnical and structural aspects, and the evaluation of lifelines in the affected area. Furthermore, the authors provide initial recommendations for improving disaster management, evaluating building stock, prioritizing urban transformation, strengthening infrastructure systems, addressing soil-building interaction issues, ensuring security measures during search and rescue efforts, utilizing satellite imagery effectively, considering seismic effects on water infrastructure, and taking a holistic approach to earthquake effects in industrial facilities.

Keywords Building damage assessment · Fault rupture and modeling · Lifelines · Local site conditions · Liquefaction

✉ Selcuk Toprak
stoprak@gtu.edu.tr

1 Department of Civil Engineering, Gebze Technical University, Kocaeli, Turkey

2 Department of Civil Engineering, Pamukkale University, Denizli, Turkey

3 Gelisim Vocational School, Istanbul Gelisim University, Istanbul, Turkey

4 Department of Remote Sensing and GIS, University of Tabriz, Tabriz, Iran

1 Introduction

On February 6th, 2023 at 4:17 local time a magnitude M_w7.7 earthquake occurred in Pazarcik district of Kahramanmaras province with a depth of approximately 8.6 km (Disaster and Emergency Management Authority Presidential of Earthquake Department—AFAD 2023). According to the primary analyses, at least three different segments totaling about 350 km long have ruptured together (USGS NEIC 2023; Garini and Gazetas 2023). Eleven minutes after this earthquake, at 4:28, a magnitude M_w6.6 aftershock occurred in a region close to the center of the first earthquake. While the earthquake activity in the region continued, approximately 100 km north of the main shock at 13:24 local time a magnitude M_w7.6 earthquake occurred in Ekinozu-Kahramanmaras province with a depth of about 7 km (AFAD 2023) and created a fracture of approximately 170 km in length (Garini and Gazetas 2023). Those earthquakes occurring on the East Anatolian Fault Zone (EAFZ), one of the most active fault zones in Turkiye, have caused losses of life and property not only in the center provinces but also in Adana, Adiyaman, Diyarbakir, Elazig, Hatay, Kilis, Osmaniye, Malatya and Sanliurfa. More than 50,000 lives were lost in 11 provinces. Additionally, on February 20th, 2023 at 20:04 local time a magnitude M_w6.4 earthquake with a depth of 21.7 km occurred in Defne district, the center of Hatay province. During this earthquake, six more people lost their lives.

This paper describes the field observations organized by MARTEST (Marmara Research and Education Center for Disaster Resistant Communities) following the occurrence of earthquakes. The observations not only encompass seismological data but also document the damage incurred by both underground and above ground structures, which provide insight into the scale of the earthquake disaster. Numerous instances were observed where ground effects such as liquefaction, rock falls, and road damage had a significant impact on structures and transportation within the affected area. The fault lines often intersected highways, roads, and railways, impeding rescue operations. Due to extensive building collapses, the number of casualties and injuries was alarmingly high, resulting in lengthy rescue operations involving both national and international teams. The paper discusses various types of structural damage caused by earthquakes and provides several examples to illustrate the effects of soil conditions. Specifically, instances of soil liquefaction problems were observed in Golbasi, Adiyaman, and Iskenderun districts of Hatay. The paper also presents an analysis of the geology and tectonics of the affected area, the strong motion characteristics of the earthquakes, and the distribution of ground motion parameters, including surface deformations using remote sensing. Additionally, the study examines the geotechnical and structural aspects as well as the evaluation of lifelines in the impacted region.

1.1 Geology and tectonics

Anatolian Plate, which holds tectonic processes that are intriguing, has a topography shaped between the North Anatolian Fault Zone (NAFZ) and the East Anatolian Fault Zone (EAFZ). Studies conducted on the Anatolian Plate specifically have revealed the existence of the westward movement of the region and the pull-apart basins formed (Reilinger et al. 2006; Sengor et al. 1985; Kocyigit and Beyhan 1998). The Anatolian Block has been moving WSW directed under the compressive effect of the Arabian and African Plates since the Miocene. The Anatolian Plate is bordered by two main fault zones. The EAFZ located in the south is approximately 500 km long and was mapped in the twentieth century (Arpat and Saroglu 1972, 1975; Ambraseys 1970; McKenzie 1976) (Fig. 1). EAFZ forms the eastern and southeastern borders of the Anatolian Plate and merges with NAFZ at Karliova (Bingol) (Arpat 1971; Arpat and Saroglu 1972, 1975). The southern border of the EAFZ connects with the Dead Sea Fault (DSF) at Samandag (Hatay) (Allen 1969, 1975; Arpat and Saroglu 1975; Rotstein 1984). From northeast to southwest, the arms of the EAFZ are Karlıova-Bingol (65 km long), Palu-Hazar (50 km long), Hazar-Sincik (85 km long), Celikhan-Golbasi (50 km long), Golbasi-Turkoglu (dip-slip component, 90 km long) and Turkoglu-Antakya (dip-slip component eastward, 145 km long) (Italiano et al. 2013). Some researchers have determined that some of these are separated by pull-apart basins (Cetin et al. 2003), some are filled with young sediments (Duman and Emre 2013) and some have acquired a transpressional character causing certain sections to become oblique (Kop et al. 2014). EAFZ is also the plate boundary that holds the Bitlis-Zagros suture zone, which is the result of the Anatolian Plate being compressed from the northwest by the Arabian Plate (Cetin et al. 2003; Reilinger et al. 2006). Global Positioning System studies conducted in the region have revealed that the EAFZ is moving westward at 6 mm/year in the northeast of Kahramanmaras and 10 mm/year in the southwest (McClusky et al. 2000; Reilinger et al. 2006; Aktug et al. 2016), with a total offset of 20–30 km. Recently, the EAFZ was broken by the Mw6.8 Sivrice-Elazig earthquake of January 24, 2020. Earthquakes that occurred

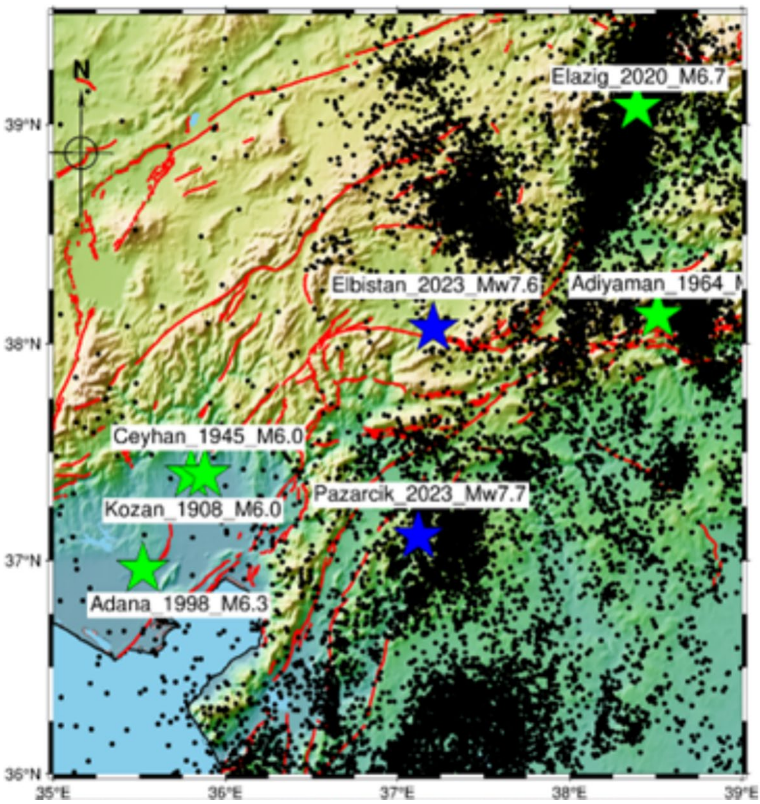

Fig. 1 Blue stars represent Feb. 6, 2023 Kahramanmaras earthquakes while green stars represent moderate earthquakes occurred in the twentieth century

in the nineteenth and twentieth centuries have caused large surface ruptures (Duman and Emre 2013). Historical earthquake seismicity in the region depicts that, in the years 1114 and 1513 Pazarcik Segment was active and Northeast and southwest branches of this segment were intensely active in the 1800s (Ambraseys 1989, 2009).

On the EAFZ, two separate earthquakes occurred at 01:47 local time on February 6, 2023, Mw7.7 located in Pazarcik-Kahramanmaras, and about 9 h later, Mw7.6 located in Elbistan-Kahramanmaras (AFAD 2023). These two earthquakes caused destructive damage in 11 cities (Kahramanmaras, Gaziantep, Malatya, Adiyaman, Hatay and Osmaniye), affected more than 13 million people and resulted in more than 50 thousand dead. After these earthquakes, more than 9000 aftershocks with magnitudes greater than 3 were recorded in the first 13 days (Kandilli Observatory and Earthquake Research Institute (KOERI), 2023) (Fig. 2). When the aftershock magnitudes are examined, a linear decrease is observed over time, which is similarly reflected in the number of aftershocks (Fig. 3). A total of 4869 earthquakes of magnitude equal to or less than 2.9, 2035 earthquakes of magnitude between 3.0 and 3.9, 409 earthquakes of magnitude between 4.0–4.9 and 50 earthquakes of magnitude greater than 5.0 were recorded (Last access date February 21, 2023). The magnitude-earthquake number graphs for the earthquakes that occurred after the 06 February 2023 Mw7.7 Pazarcik-Kahramanmaras earthquake until 21 February 2023 are given. An earthquake with a magnitude of Mw6.4 (AFAD 2023), occurred at 20:04 local time on February 20, 2023, in the Samandag district of Hatay Province.

The first earthquake broke the Erkenek, Pazarcik, and Amanos fault segments of the Dead Sea Fault Zone (DAFZ), resulting in a rupture along a 330 km line that intermittently surfaced in some areas (USGS 2023). During on-site field observations, surface ruptures were observed in Goksun, Golbasi, Turkoglu, Sekeroba, Nurdagi, and Islahiye. Aerial photographs were taken using a drone, and surface modeling was performed to measure the

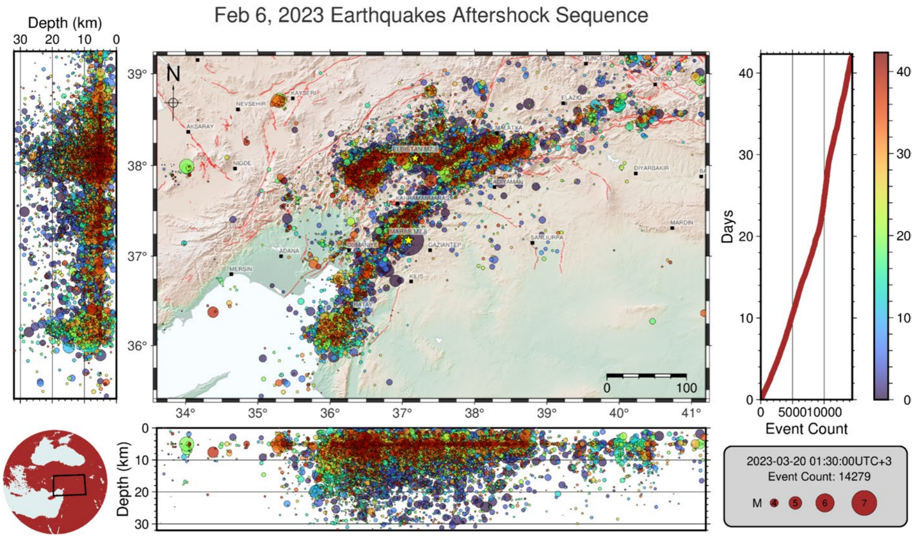

Fig. 2 Depth section distribution of earthquakes occurred until 26th February 2023 UTC:00 after the 06 February 2023 M_w7.7 Pazarcik (Kahramanmaras) earthquake (KOERI). Active fault zones are shown as red lines on the map (Emre et al. 2013)

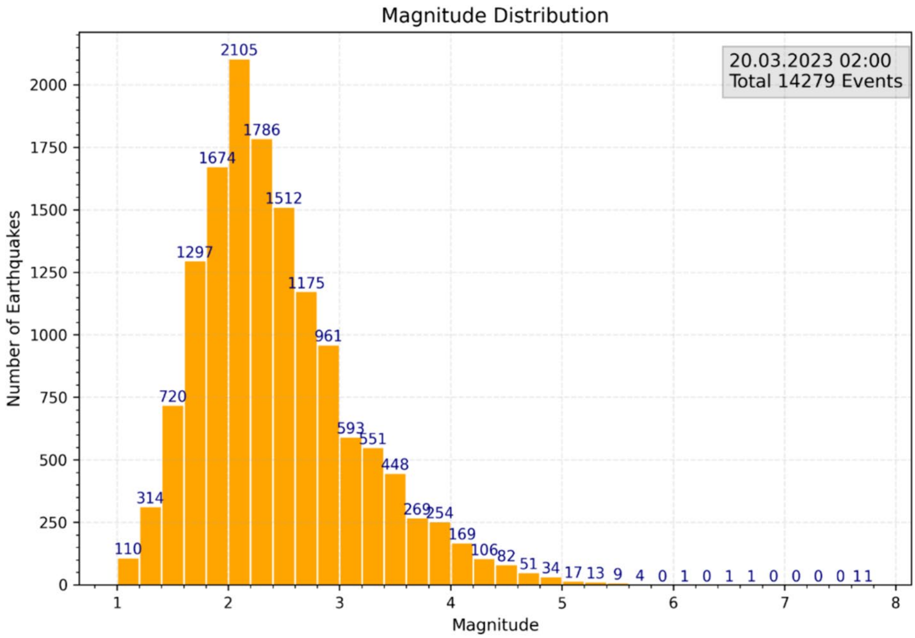

Fig. 3 Distribution of earthquake magnitude and number of earthquakes occurred until February 21, 2023, following the Mw7.7 Pazarcik (Kahramanmaras) earthquake on February 6, 2023 (KOERI 2023)

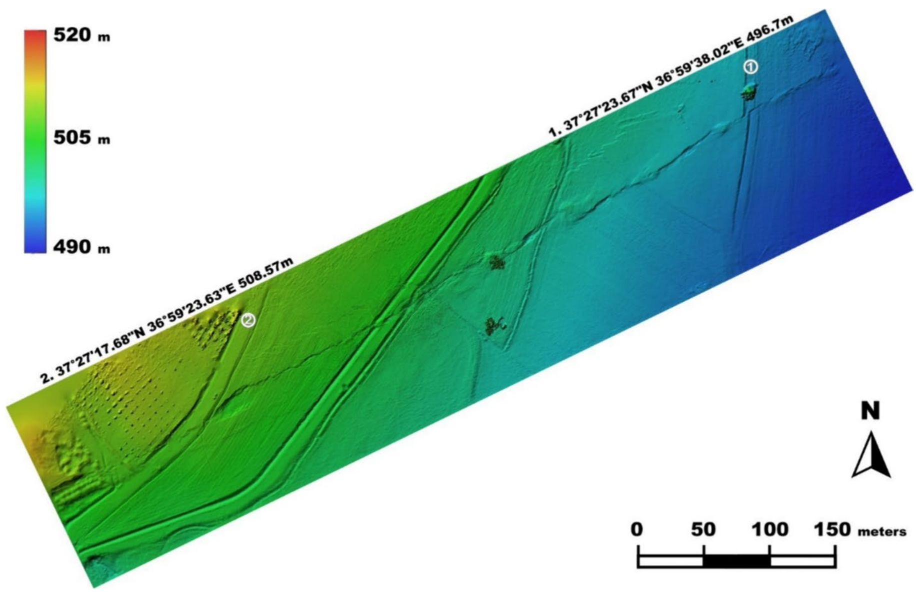

Fig. 4 Depiction of fault surface rupture modeling using drone imagery in the Sekeroba region

displacement range (Fig. 4). The drone modeling study conducted in Sekeroba measured the highest displacement at 4.13 m. This Mw7.7 earthquake exhibited a left-lateral strike-slip fault mechanism consistent with the characteristics of the DAFZ fault system.

2 Strong ground motion characteristics

The Pazarcik Mw7.7 earthquake that occurred on February 6, 2023 at 04:17 local time and the Elbistan Mw7.6 earthquake that occurred at 13:24 were recorded by AFAD and KOERI stations located in the region. After the earthquakes, digital data belonging to certain seismic recorders were obtained in ASCII (*.asc) format via a web page, which were provided by AFAD-TADAS by accessing the acceleration records (last accessed on February 16, 2022). Figure 5 shows the locations of the strong ground motion stations used in this study.

The characteristics of strong ground motion records from 21 seismic recorders, which recorded a maximum ground acceleration of 350 gal or more during the Mw7.7 earthquake, are presented alongside the data listed in Table 1. The values presented in this study and listed in the table were calculated using the analytical methods outlined by Tugsal and Mutlu (2023). For each earthquake, time histories of acceleration, velocity, and displacement were generated. Additionally, Arias intensities (Arias 1970) and frequency content (Fourier Amplitude-Frequency graphs) of the time series were calculated. The signals obtained from the recorders underwent Fourier transformation to evaluate the frequency

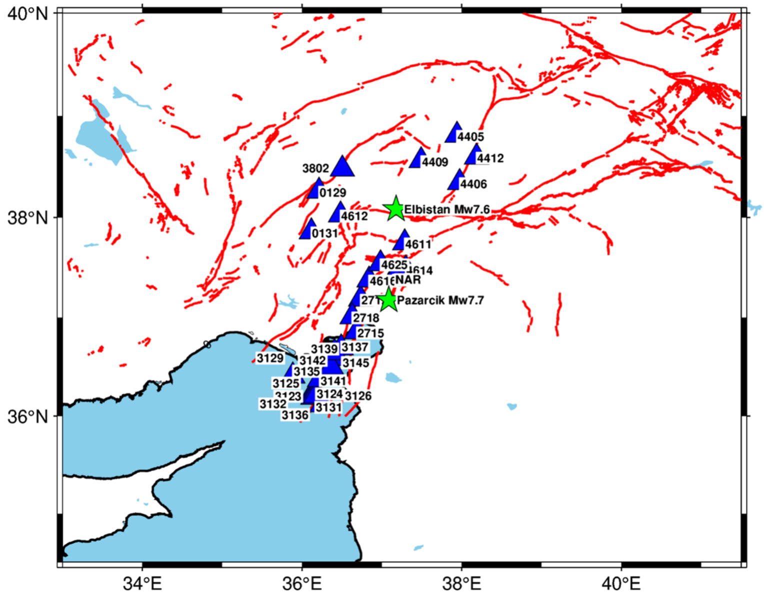

Fig. 5 Distribution map of strong ground motion stations used in the study. Active fault zones are shown as red lines on the map (Emre et al. 2013)

Table 1 Strong Ground Motion Stations and Their Measured Acceleration Values

Station information									AFAD database			This study		
Station Code	Latitude	Longitude	City	District	R_{epi} (km)	R_{hyp} (km)	V s,30 (m/s)	Soil Class	PGA_NS (cm/s^2)	PGA_EW (cm/s^2)	PGA_UD (cm/s^2)	PGA_NS (cm/s^2)	PGA_EW (cm/s^2)	PGA_UD (cm/s^2)
3129	36.1343	36.1912	Hatay	Defne	146.39	146.64	447.0	ZC	1350.49	1207.62	707.55	1350.50	1207.60	707.60
3126	36.1375	36.2202	Hatay	Antakya	143.54	143.80	350.0	ZD	1211.04	1030.18	1071.45	1186.60	999.10	945.70
3141	36.2197	36.3726	Hatay	Antakya	125.42	125.71	338.0	ZD	961.12	868.82	722.66	991.80	835.80	668.30
3125	36.1326	36.2381	Hatay	Antakya	142.15	142.41	448.0	ZC	822.62	1121.95	1151.56	772.70	1072.00	1055.50
3135	35.8831	36.4089	Hatay	Arsuz	142.15	142.41	460.0	ZC	740.97	1372.07	588.97	741.10	1314.70	574.90
2718	36.6266	37.0078	Gaziantep	islahiye	48.30	49.06	–	–	702.42	644.97	585.79	650.60	624.80	584.20
3123	36.1597	36.2142	Hatay	Antakya	143.00	143.26	470.0	ZC	655.57	593.94	867.58	651.90	581.40	840.50
4616	36.8384	37.3755	Kahramanmaras	Tűrkoglu	20.54	22.27	390.0	ZC	652.76	502.87	397.27	664.30	488.30	387.70
3142	36.3661	36.4980	Hatay	Kinkhar	106.49	106.84	539.0	ZC	646.63	749.51	505.89	635.60	735.80	470.10
NAR	37.1574	37.3919	Kahramanmaras	Pazarcik	15.35	17.60	–	–	646.50	578.80	398.66	646.50	578.80	398.70
3145	36.4064	36.6454	Hatay	kirikhan	91.13	91.54	533.0	ZC	600.04	696.39	663.18	589.90	693.10	609.30
4615	37.1380	37.3868	Kahramarmaras	pazarcik	13.83	16.28	484.0	ZC	537.74	556.46	664.58	587.70	556.50	664.60
3139	36.4144	36.5838	Hatay	Kinkhar,	96.19	96.57	272.0	ZD	577.13	504.82	378.62	572.90	504.10	353.30
3124	36.1722	36.2387	Hatay	Antakya	140.11	140.37	283.0	ZD	572.63	638.32	578.08	568.80	618.70	579.10
2712	36.7328	37.1840	Gaziantep	Nurdagi	29.79	31.01	–	–	554.85	602.66	346.12	551.50	588.50	315.30
3136	36.2472	36.1159	Hatay	Altinözű	148.38	148.63	344.0	ZD	534.22	401.97	220.46	518.00	382.60	218.40
3132	36.1716	36.2067	Hatay	Antakya	143.12	143.38	377.0	ZC	515.31	514.63	354.18	500.90	507.70	356.20
2715	36.6856	36.8554	Gaziantep	islahiye	57.62	58.25	–	–	456.12	340.76	263.92	373.90	298.10	166.50
3137	36.4885	36.6929	Hatay	hlassa	82.48	82.93	688.0	ZC	453.09	848.01	501.98	425.60	747.30	446.20
4625	36.9819	37.5387	Kahramanmaras	Dulkadiroglu	28.40	29.67	346.0	ZD	448.15	483.65	367.37	447.00	469.50	352.10
3131	36.1633	36.1912	Hatay	Antakya	144.93	145.23	567.0	ZC	363.03	366.05	153.96	355.50	354.80	146.40

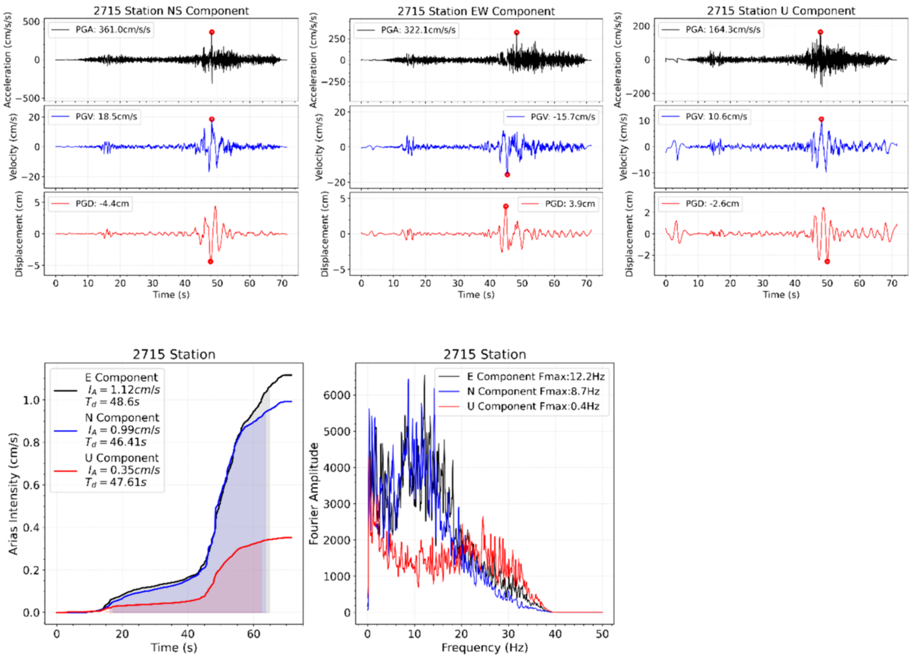

Fig. 6 The characteristic features of strong ground motions recorded at station code 2715 during the Pazarcik M_w7.7 earthquake

content. Dominant frequency calculations were performed using the geometric averages of the horizontal and vertical components, as shown in Fig. 6.

Analyses were conducted to calculate different receiver, source, and software-dependent soil conditions and amplification values, with the results compared accordingly. The horizontal-vertical spectral ratio (HVSR) method (Nakamura 1989; Lermo and Chavez-Garcia 1993) was employed to determine soil dominant frequency values. Furthermore, response spectras were obtained from records taken at stations located in different soil conditions to evaluate the earthquake load on structures and assess regional damage.

2.1 Spectrum characteristics

The response spectra of the strong ground motion records obtained from each station, corresponding to their coordinates, have been compared with the horizontal and vertical elastic design spectra defined in the Turkish Building Earthquake Code (TBDY 2018) for two different local soil classes, as shown in Fig. 7. Examination of the results from the strong ground motion recordings at each station reveals that the spectral accelerations at stations 4625, NAR, and 3136 are close to the design earthquake with a 475-year return period, corresponding to a 10% probability of exceedance in 50 years. An amplification effect, especially in the period range of medium–high structures, is observed at stations 2712, 3124, and 3139. The response spectra from recordings at other stations indicate particularly high spectral acceleration values in the short period range.

The characteristics of the strong ground motion recordings, which were recorded at 10 seismic stations where the maximum ground acceleration for the M_w7.6 Elbistan

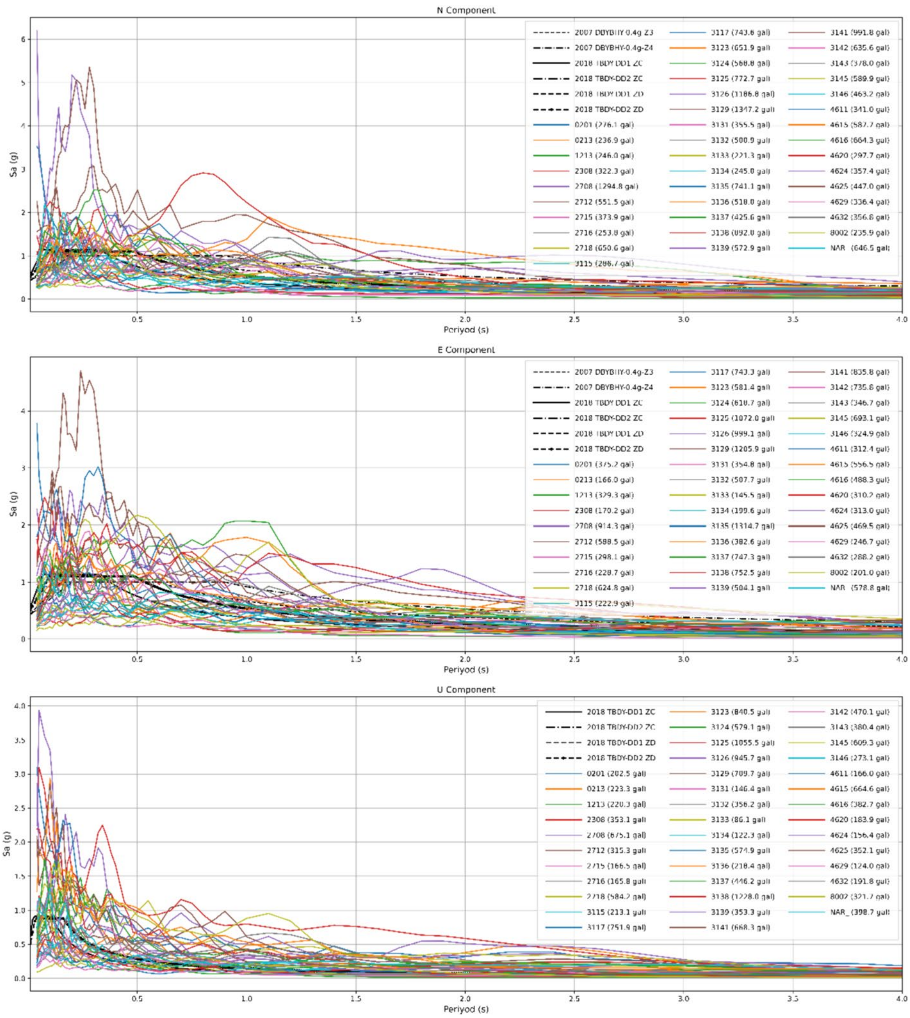

Fig. 7 Comparison of the response spectra of strong ground motion records from the M_w7.7 Pazarcik earthquake on February 6, 2023 with the design spectra defined in TBDY (2018)

Earthquake was recorded as 150 gal or higher, are shown in Table 2 together with the characteristics of the recorded strong ground motion. The values presented in this study and listed in the table were calculated using the analytical methods outlined by Tugsal and Mutlu (2023). Figure 8 shows the characteristics of strong ground motions recorded at TK0129 station during the Elbistan M_w7.6 earthquake.

Figure 9 shows the response spectra of strong ground motion records obtained from each station, corresponding to their coordinates, for three different local soil classes, compared with the horizontal and vertical elastic design spectra defined in TBDY (2018). DD1 represents the design earthquake with a 2% probability of exceedance in 50 years and a return period of 2475 years, while DD2 represents the design earthquake with a 10% probability of exceedance in 50 years and a return period of 475 years.

Table 2 Characteristics of the M_w7.6 Elbistan Earthquake acceleration recorders and strong ground motion recordings

Station information									AFAD Database			This study		
Station Code	Latitude	Longi-tude	City	District	R_{epi}(km)	R_{hyp} (km)	$V_{S,30}$ = (m/s)	Soil Class	PGA_ NS (cm/s^2)	PGA_ EW (cm/s^2)	PGA_UD (cm/s^2)	PGA_ NS (cm/s^2)	PGA_ EW (cm/s^2)	PGA_ UD (cm/s^2)
4612	36.4819	38.0240	Kahramanmaras	Göksun	66.68	67.05	246.0	ZD	635.45	523.21	494.91	627.20	520.70	430.20
4406	37.9738	38.3439	Malatya	Akcadag	70.17	70.52	815.0	ZB	467.20	409.31	318.75	444.70	382.50	284.90
0131	36.1153	37.8566	Adana	Saimbeyli	101.83	102.07	–	–	402.32	331.69	85.29	404.20	325.00	84.50
4409	37.4908	38.5606	Malatya	Darende	56.86	57.28	–	–	287.04	218.04	124.28	252.10	193.80	85.90
3802	36.5036	38.4781	Kayseri	Sariz	77.41	77.73	305.0	ZD	195.79	220.88	122.81	193.10	217.70	119.80
4611	37.2843	37.7472	Kahramanmaras	Caglayancerit	38.21	38.85	731.0	ZC	194.40	139.04	72.57	192.30	133.50	71.30
4614	37.2978	37.4851	Kahramanmaras	Pazarcik	67.35	67.71	671.0	ZC	160.82	206.05	89.21	160.50	197.60	80.20
4412	38.1839	38.5969	Malatya	Yazihan	99.89	100.14	–	–	159.03	126.38	79.90	157.80	126.00	79.00
4405	37.9396	38.8107	Malatya	Hekimhan	100.81	101.05	579.0	ZC	155.41	158.05	121.88	147.60	151.60	125.30
0129	36.2109	38.2592	Adana	Tufanbeyli	91.84	92.11	965.0	ZB	154.46	172.18	83.75	150.40	163.70	82.80

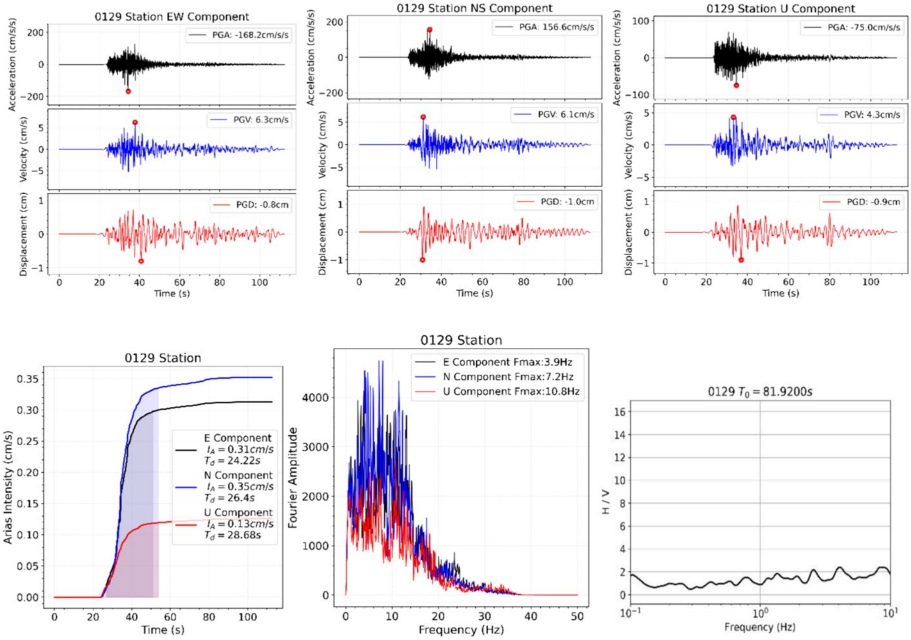

Fig. 8 Characteristics of the strong ground motion recorded at TK0129 station

3 Surface deformation by using remote sensing

To assess ground deformation and the extent of damage in the affected area, three synthetic aperture radar (SAR) images from the ascending orbit (T14) of the Sentinel-1 satellite were acquired on 2023.01.16, 2023.01.28, and 2023.02.09. The pre-event (2023.01.28) and post-event (2023.02.09) images, with a 12-day interval, were used for interferogram generation in single look complex (SLC) format. It should be noted that, due to the short temporal gap between these two events, secular deformation for each event cannot be distinguished in 12-day interferograms. During the SAR interferometry (InSAR) process, the topographic phase component was reduced using a 90 m digital elevation model (DEM) from the Shuttle Radar Topography Mission (SRTM) (Farr et al. 2007). Speckle noise was reduced through a multilooking process for all the SLC images, with azimuth and range looks for a 20 m ground resolution set to 1 and 5, respectively. Figure 10 shows the deformation map of the study area after the Mw 7.7 and Mw 7.6 earthquakes, with the observed maximum deformation being about 4 m, though field observations suggest it might be even greater.

For generating a damage proxy map, coherence-based methods from previous studies were utilized (Karimzadeh et al. 2017; Hajeb et al. 2020; Karimzadeh and Matsuoka 2018a, 2018b). As illustrated in Fig. 11a, multitemporal damage assessment requires at least three SAR images, with two taken before the events (Hajeb et al. 2020). Assuming the image from 2023.01.28 as a nodal image connecting the other two images, sequential InSAR analysis was performed for the master and slave images, generating the pre-seismic and co-seismic coherence products shown in Fig. 11b. The natural break classification method was used to reclassify the differential coherence map into a preference

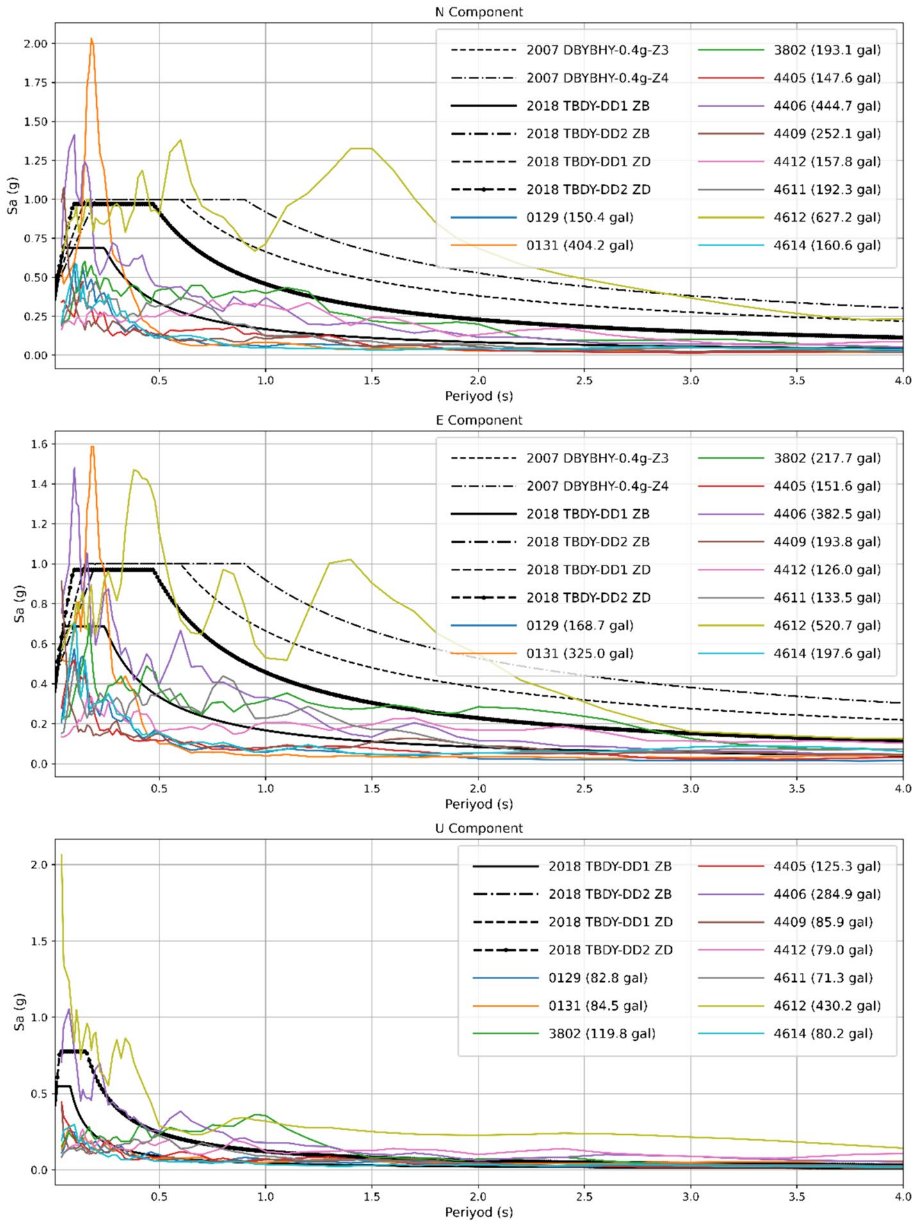

Fig. 9 Comparison of the response spectra of strong ground motion records recorded at 10 stations during the February 06, 2023 Mw7.6 Elbistan earthquake with the TBDY (2018) design spectra

scale map, aiming to optimally arrange values across various classes. This approach minimizes the average deviation within each class relative to its mean while maximizing the deviation from other classes. All maps were then reclassified into seven classes (negligible damage, two positive moderate damage, two negative moderate damage, one positive high damage, one negative high damage) based on experiences from previous

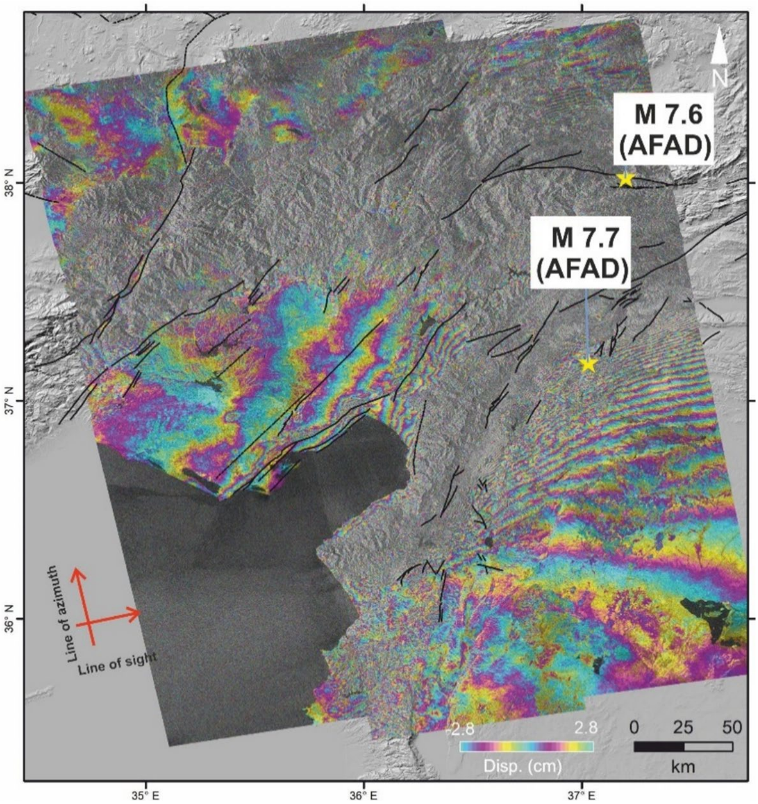

Fig. 10 Initial 12-day interferogram of the Maras earthquakes from ascending orbit (T14). Yellow stars are the location of the epicenters, black lines are the fault lines

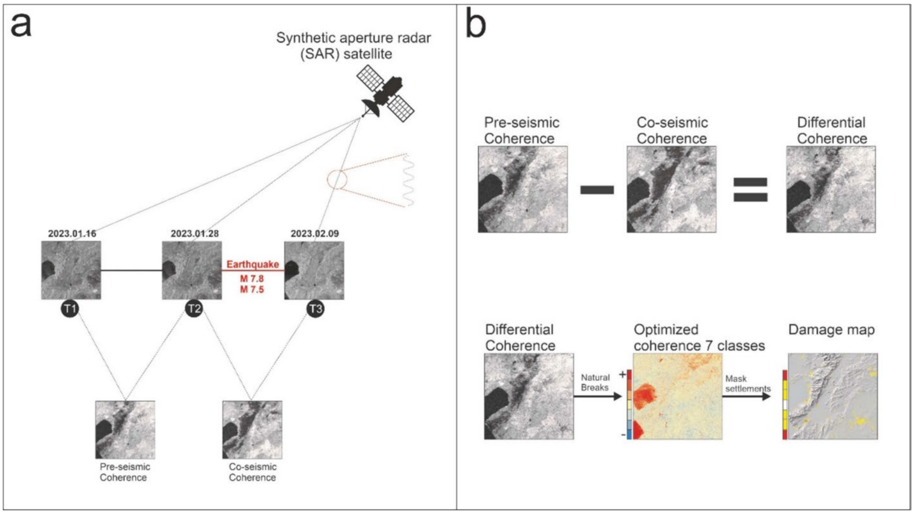

Fig. 11 a Schematic illustration of multitemporal damage identification by using InSAR coherence analysis; b differential coherence map and coherence optimization method (natural breaks)

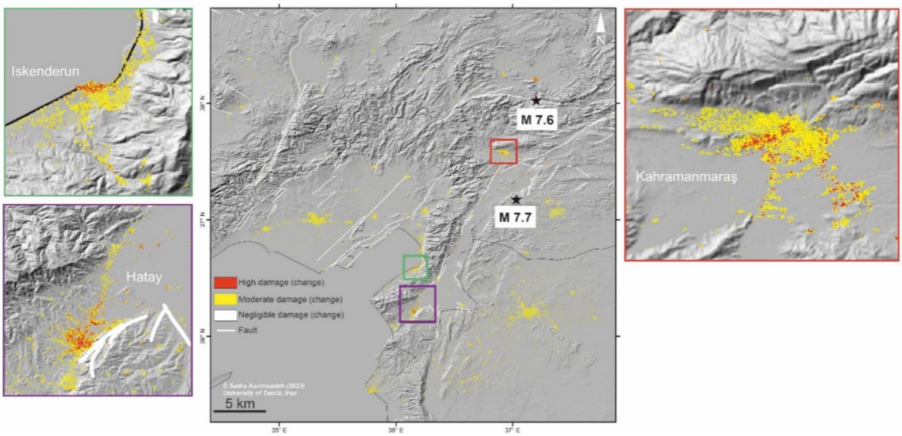

Fig. 12 Damage map of the affected area extracted from multitemporal coherence analysis of three Sentinel-1 images

earthquakes (Karimzadeh et al. 2017; Hajeb et al. 2020; Karimzadeh and Matsuoka 2018a, 2018b). Figure 12 shows the extent of damage in the affected area, covering approximately 90,000 km^2, with heavy damage observed in urban areas such as Kahramanmaras, Iskenderun, Antakya, and Elbistan.

4 Ground motion parameters distribution

The ground motion parameters (MMI, PGA, PGV, Sa) for the February 6th Mw7.7 Pazarcik Earthquake have been calculated and are presented in Figs. 13, 14a, b, c, and d, respectively. The USGS ShakeMap approach, as described in the ShakeMap 4 Manual (Worden et al. 2023), was applied. The earthquake region was subdivided into grids, with a phantom station located in the center of each grid at 10 km spacing. Ground motion parameters were estimated at the phantom stations using the ground motion models of Boore and Atkinson (2008) and Chiou and Youngs (2014), each weighted equally. Local soil conditions were considered using the $V_{s,30}$ values in the proposed ground motion models, with topographic-slope-based $V_{s,30}$ map values (Heath et al. 2020) utilized for the region. Interpolation was carried out among the estimated ground motion values at the phantom stations, and adjustments were made using recorded station data.

In estimating the ground motion parameters PGA, PGV, Sa (0.2 s), and Sa (1.0 s), the NGA ground motion models of Boore and Atkinson (2008) and Chiou and Youngs (2014) were used with equal weighting. For intensity distribution, regression relationships between Modified Mercalli Intensity (MMI) and PGA or PGV developed by Wald et al. (1999) were applied. Figure 13 shows the MMI distribution for the region. The red regions indicate IX and IX + intensity, consistent with field observations in Islahiye, Nurdagi, Sekeroba, Turkoglu, Antakya, and Golbasi. Kahramanmaras and Adiyaman city centers experienced intensities of VII and VIII, while Gaziantep city center experienced intensity VII.

Figure 14a shows the PGA distribution in the region, with values greater than 0.4 g distributed along the fault line, indicating extensive damage. Figure 14b shows the PGV distribution, with values higher than 140 cm/s along the fault line in the epicentral region.

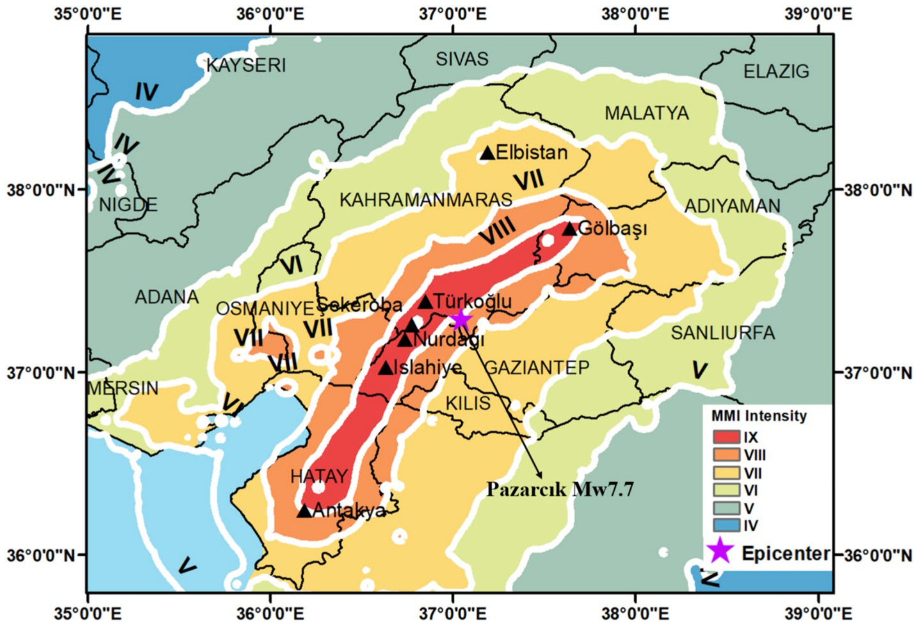

Fig. 13 Intensity distribution of the February 6th Mw7.7 Pazarcik Earthquake

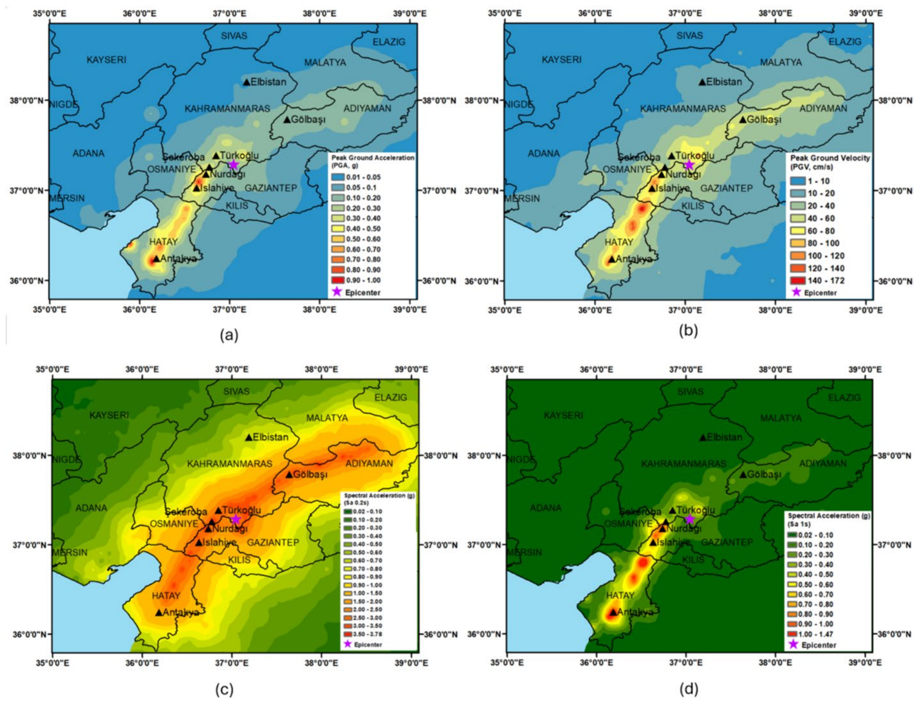

Fig. 14 For February 6th Mw7.7 Pazarcik earthquake, distributions of **a** PGA distribution **b** PGV **c** the spectral acceleration at T = 0.2 s period **d** the spectral acceleration at T = 1.0 s period

Figure 14c displays the spectral acceleration values in the short-period region (T = 0.2 s), exceeding 2.0 g, which is higher than TBDY (2018) design spectra values for the same period, indicating potential damage to low-rise buildings along the fault line. Figure 14d shows the spectral acceleration in the longer period region (T = 1.0 s), exceeding 0.8 g, also higher than TBDY (2018) design spectra values for the region.

5 Geotechnical aspects

Previous earthquake observations worldwide have established that local site conditions significantly influence the behavior and damage sustained by structures. Notable earthquakes, such as those in Mexico City (1985), Loma Prieta (1989), Kocaeli (1999), Christchurch (2011), and Kumamoto (2016), have demonstrated that local site conditions are crucial factors affecting the amplitude parameters and response spectra of earthquakes. After the Kahramanmaras earthquakes, initial investigations in the affected area revealed the significant impact of local site conditions. Geotechnical issues identified during site observations included liquefaction, liquefaction-induced lateral spreading and displacements, landslides, slope failures, and rockfalls. Although further investigations will determine the extent, site amplifications were notably prominent at many alluvial sites in the region, such as Golbasi, Iskenderun, and Antakya. In earthquake-affected areas, various foundation problems were identified. Figures 15a, b, and c show building rotations and differential settlements observed in Golbasi and Adiyaman. The figures also highlight the settlements and upheavals of the pavement along Malatya-Kahramanmaras street passing through Golbasi.

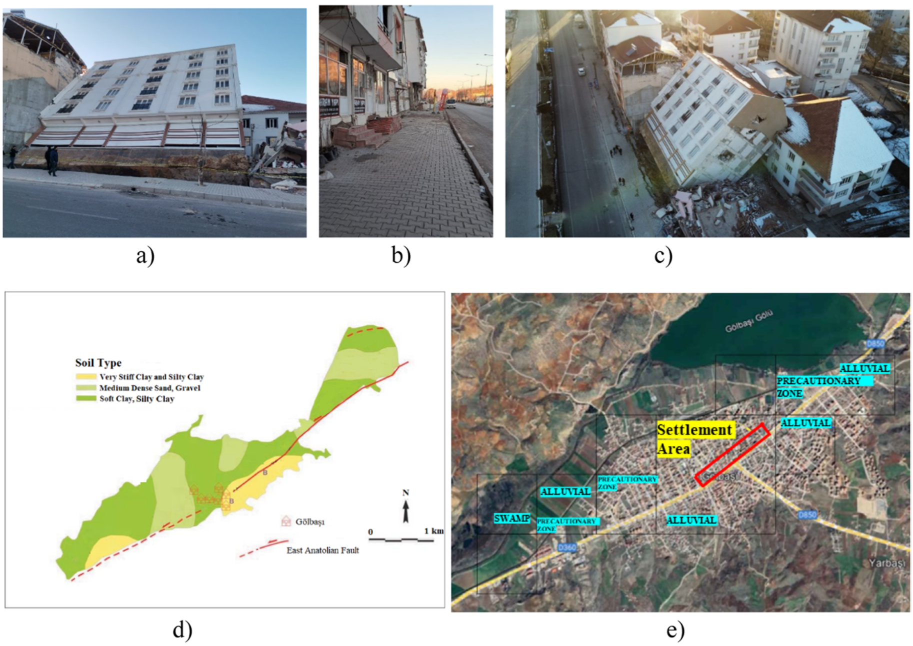

Fig. 15 Problems observed in foundations **a**, **b**, and **c** in different soil types **d** in Golbasi, Adiyaman **e** (**d** and **e**, modified from Akil et al. 2008)

The Golbasi province is characterized by two distinct soil zones: alluvial soil deposits and swamp soil deposits (Akil et al., 2008). The Kahramanmaras earthquake resulted in settlements and upheavals in the alluvial area. Analysis of the soil group distribution map (Fig. 15d) reveals that the southeastern part of the district is predominantly composed of very stiff, highly plastic clay material, while the district as a whole consists mostly of fine-grained, low-plasticity soft clay and medium-density sandy material. The water table fluctuates between 0.65 m and 3.50 m. According to studies conducted by Akil et al. (2008), the groundwater level is high, and there is a moderate risk of liquefaction, particularly in sandy and some gravelly areas. These areas are susceptible to liquefaction, which can lead to surface damage. Given the high groundwater level, presence of alluvial soils, moderate liquefaction risk levels, and the district's location in an earthquake zone, these areas have been classified as precautionary zones (Fig. 15e). The Kahramanmaras earthquakes resulted in significant surface and structural damage in the alluvial soils in these designated precautionary zones.

In Kahramanmaras, soil conditions and shear wave velocity vary greatly throughout the city center (Sandal and Karademir 2013; Naji et al. 2020). The $V_{s,30}$ distributions show the presence of different soils ranging from soft soils to rock. It is evaluated that these varying soil conditions, together with structural properties, affect the damage distribution. Antakya was one of the severely affected locations, with more than half of the structures in the city damaged. Figure 16 illustrates different geological sections and elevations obtained from drillings in the city center of Hatay/Antakya. In a study conducted by Over et al. (2011), SW-NE, NW–SE, and SW-NE soil sections were extracted using 17 shallow borehole data in the city center of Antakya. According to these sections, the soil in Antakya generally consists of Quaternary materials such as clay, gravel, and alluvial sands.

Another area that experienced significant damage in Hatay is Iskenderun. Figure 17 shows a typical soil profile for Iskenderun and the effects of liquefaction on buildings and roads. A sample soil profile was defined using two soundings made in the Konarli District of Iskenderun (Toktanis and Over 2021). Intense sand and silt units were observed. During reconnaissance studies, serious damage was observed on buildings and roads along Ataturk Boulevard (Figs. 17b and c). The rainwater collection system in the area was damaged by liquefaction and was rendered unusable after the earthquake (Fig. 17b). Settlement was observed in buildings along the route, and significant lateral spreading was also noted (Fig. 17c).

5.1 Liquefaction and lateral spreading cases

Soil liquefaction is defined as a significant reduction in the shear strength and stiffness of saturated cohesionless or low cohesive soils, following an increase in pore water pressure under earthquake shaking. Field observations in the earthquake zone revealed lateral spreading and settlements caused by liquefaction. Additionally, a large amount of liquefied soil material surfaced due to liquefaction. Figure 18 shows the sand boils and lateral spreading along the coast resulting from liquefaction in Iskenderun, Hatay. Intense liquefaction features were detected on the surface along Ataturk Boulevard (Figs. 17b and c). These observations are important for evaluating parameters such as the liquefaction potential index (LPI) and the liquefaction severity index (LSN), which are frequently used in engineering applications (e.g., Toprak and Holzer 2003; Toprak et al. 2019).

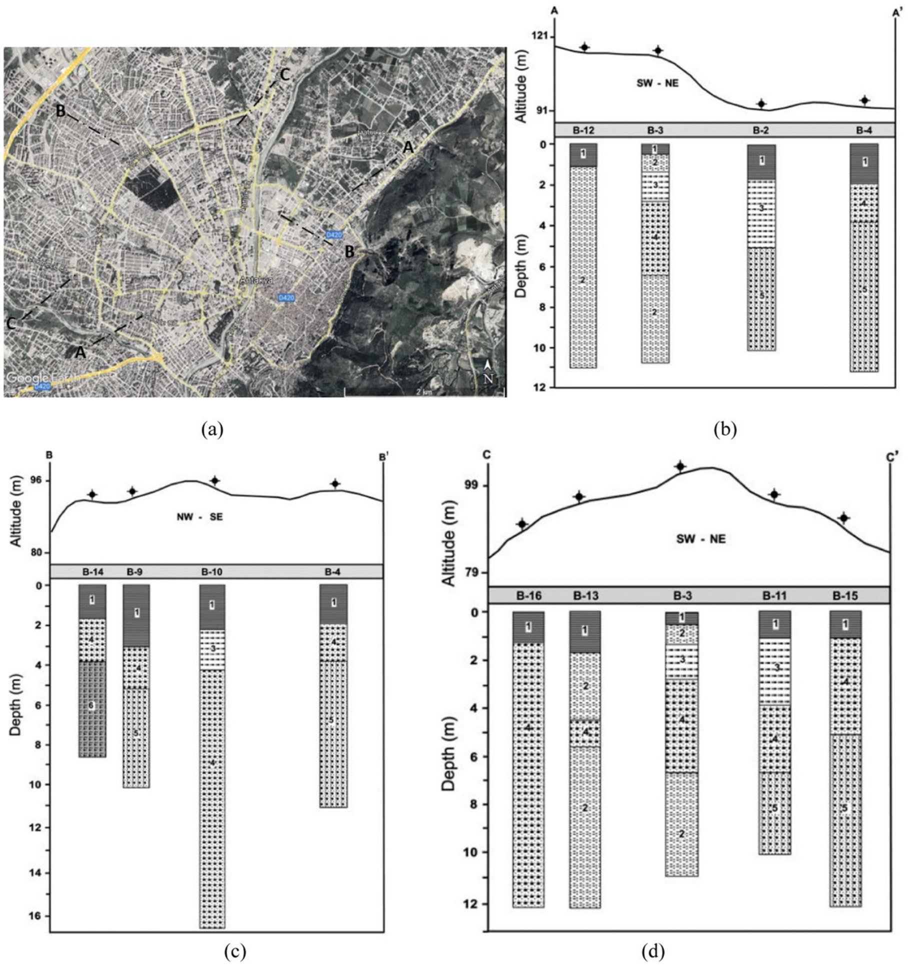

Fig. 16 Hatay/Antakya **a** Boring locations, **b** A-A' section **c** C–C' section **d** B-B' section soil profile (Over et al., 2010) ((1) Fill, (2) Silty sandy clay, (3) Sandy clayey silt (4) Silty sand, (5) Gravel clayey silty sand, (6) Clay sandy gravel)

5.2 Slope instability and rock falls

Slope failures and rockfalls occurred at many locations in the region, with some landslides causing damage to structures and lifelines. Figure 19 shows examples of landslides observed in earthquake-affected areas. The landslide in Gaziantep/Sahinbey (Fig. 19a) also puts surrounding structures at risk. Many small shops at the bottom of the hill face immediate landslide risks, prompting evacuation procedures following the earthquake. Similar instances, such as the one shown in Fig. 19b, were encountered in different regions along the investigation route. Road closures occurred in these areas immediately after the earthquake, but the roads were reopened after clearing the rocks and making some repairs. However, due to the potential for additional slope movements triggered by subsequent tremors or precipitation, ongoing monitoring and precautionary measures are necessary.

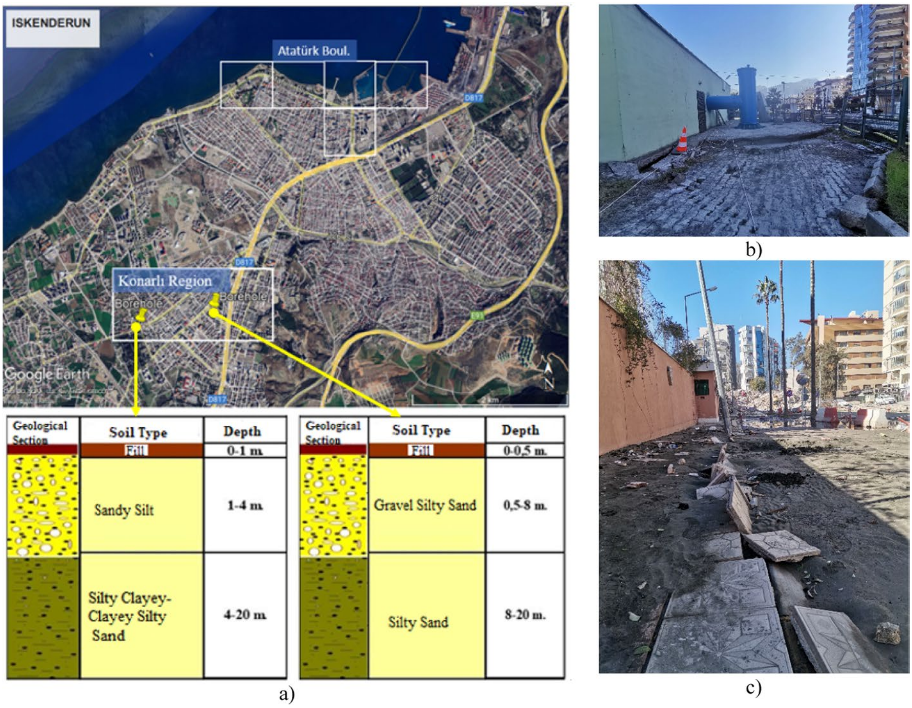

Fig. 17 Damages along the Ataturk Blvd in Iskenderun and typical soil profile Konarli District as reported by Toktanis and Over (2021)

(a) Sand boils (b) Lateral spreading

Fig. 18 Liquefaction-induced ground deformations in Iskenderun/ Hatay

6 Structural aspects of the observed damages

More than 50,000 casualties occurred across 11 provinces along the Eastern Anatolian Fault Line, and over half a million buildings were destroyed or severely damaged, resulting in significant financial losses. Following the devastating Pazarcik Mw7.7 and Elbistan Mw7.6 earthquakes, a nine-member team consisting of civil engineering faculty members,

(a) Gaziantep/Sahinbey landslide

(b) Ekinozu landslide and rockfall

Fig. 19 Slope instability and rockfall observations

graduate students, and doctoral candidates conducted field investigations to examine the damage to infrastructure and superstructures in the most affected areas. The most severe damage was concentrated in provinces near the fault line, with significant destruction also occurring in Osmaniye, Adana, Diyarbakir, Sanliurfa, Kilis, and Elazig. The severity of the destruction in buildings was determined by several factors:

- Structural system design and construction quality deficiencies (manufacturing defects)
- Age of buildings
- Non-compliance with regulations during construction
- Intensity of ground motion (high acceleration values recorded)
- Liquefaction and bearing capacity of the soil on which foundations sit
- Different floor levels of buildings built in adjacent order

Due to significant code changes in 1998 and numerous regulatory improvements after the 1999 Kocaeli earthquake, it is appropriate to evaluate the building inventory in the region as pre- and post-2000 buildings. When examining the construction years of buildings in the regions affected by the Kahramanmaras earthquakes, more than 50% of reinforced concrete buildings were built after 2000. According to data from the Republic of Turkiye Statistical Institute and the Ministry of Interior General Directorate of Population and Citizenship Affairs—National Address Database & Spatial Address Registration

System, more than 50% of households in the total region reside in buildings constructed after 2000. The distribution of the number of damaged buildings by province is provided in Table 3, according to data from the Ministry of Environment, Urbanization, and Climate Change. The total numbers for all provinces, categorized by different damage levels, are highlighted in bold in the last row of the table.

Based on the data, about 2,300,000 people were directly affected by shelter issues following the earthquake. The ongoing seismic activity and conditions in the affected zone exacerbate the housing crisis. The estimated damage for houses that need immediate demolition, are severely damaged, or destroyed amounts to 823 billion TL. Additionally, the damage for moderately damaged houses is calculated to be 209 billion TL. Thus, the total housing damage is 1,032 billion TL, which is approximately 55 billion U.S. dollars according to the conversion rates immediately after the earthquake.

6.1 Damages to reinforced concrete buildings

The collected building data included structures with construction permits, indicating that 86.7% of the building stock in the region consists of reinforced concrete structures. While the high acceleration values recorded during the earthquakes are primarily considered the cause of structural damage, factors such as structural system design, construction defects, and lack of engineering services for reinforced concrete buildings in the region are identified as the most significant contributors to the severe damage. Upon evaluating the structural damages in the region, the following deficiencies and defects were commonly observed in buildings believed to have been constructed before 2000 (Fig. 20):

- Low concrete strength: Interviews with local administration revealed that river sand was commonly used in pre-2000 constructions, and instead of crushed stone, flat-surfaced large-grained stone fragments were used, leading to voids in the concrete.
- Use of smooth surface reinforcing steel,

Table 3 Number of Buildings Damage Assessed in the Region Affected by Kahramanmaras Earthquakes as of March 6, 2023

City	Total number of emergency + severe + collapsed houses	Number of moderately damaged houses	Number of slightly damaged houses
Adana	2952	11,768	71,072
Adiyaman	56,256	18,715	72,729
Diyarbakir	8602	11,209	113,223
Elazig	10,156	1522	31,151
Gaziantep	29,155	20,251	236,497
Kahramanmaras	99,326	17,887	161,137
Malatya	71,519	12,801	107,765
Hatay	215,255	25,957	189,317
Kilis	2514	1303	27,969
Osmaniye	16,111	4122	69,466
Sanliurfa	6163	6041	199,401
Total for the Region	**518,009**	**131,576**	**1,279,727**

Fig. 20 Problems observed in the quality of concrete and the availability of smooth surface reinforcing steel

One notable issue in the damaged structures throughout the region is the insufficient longitudinal reinforcement in the cross-sections. It was observed that transverse reinforcements were inadequately placed both along the cross-section and at the beam-column joints. Considering the low concrete quality observed in the damaged structures, the lack of transverse reinforcement to withstand shear effects has been concluded as one of the most significant reasons for the damage (Fig. 21).

- Contrary to the philosophy of earthquake-resistant building design, which emphasizes the "strong column-weak beam" approach, buildings estimated to have been constructed before 2000 often exhibited the opposite. In this incorrect application, column sections were minimized while connected to larger beams. As a result, buildings experienced intense damage due to the collapse of heavily constructed slabs, as columns failed before beams under the strong ground motion, leading to significant casualties (Fig. 22).
- Many buildings were damaged due to the irregularity of soft/weak stories, such as the relatively high design of entrance floors, the removal of infill walls for commercial

Fig. 21 Problems observed with insufficient beam-column joint details

Fig. 22 Observed design problem as strong beam-weak column

purposes, and interventions on vertical structural elements for equipment placement (Fig. 23).

- Buildings that experienced significant permanent displacement of their structural elements and partially collapsed due to the earthquake are classified as "urgently to

Fig. 23 Design problem observed as soft/weak stories

Fig. 24 Partially collapsed buildings

Fig. 25 Pounding effect observed in adjacent buildings

be demolished." These buildings are unusable, and even the evacuation of belongings is not possible (Fig. 24).

- It has been observed that buildings constructed adjacent to each other with insufficient expansion joints suffered damage because of collisions under strong ground motion. This structural irregularity, observed in adjacent buildings with different floor levels and referred to as the "Pounding Effect," can cause severe damage, even total collapse, in structures with different dynamic characteristics (Fig. 25).
- Despite the extensive damage, there are also structures in the region that survived the earthquakes without any damage (Fig. 26).

Fig. 26 Undamaged structures after the earthquake

6.2 Damages to industrial facilities

Heavy damage occurred in industrial facilities within the earthquake zone. There are three Organized Industrial Zones (OIZ) in Kahramanmaras province, and damages were observed in the factory buildings within and outside of these OIZs. Following the earthquake, businesses in many factories had to halt operations due to both structural and non-structural damages, as well as the impact on the personnel working in the facilities. The region's industrial sector is predominantly composed of the textile, mining, and food industries. The textile industry in Kahramanmaras and Adiyaman has come to a standstill. While there is no specific information regarding damage to mining facilities, the energy-producing thermal power plants in the area have become inactive, causing a cessation of production in the particular mining sector. Additionally, the earthquake's impact on the personnel and their families, along with the use of mining equipment and vehicles in earthquake search and rescue operations, has also contributed to the work stoppage in this sector. The seven thermal power plants located in or near the earthquake zone and considered important are listed below:

- Afsin-Elbistan A Thermal Power Plant with a capacity of 1355 megawatts (Kahramanmaras)
- Afsin-Elbistan B Thermal Power Plant with a capacity of 1440 megawatts (Kahramanmaras)
- Tufanbeyli Thermal Power Plant with a capacity of 450 megawatts (Adana)
- Iskenderun Thermal Power Plant with a capacity of 1308 megawatts (Adana-Yumurtalik)
- Hunutlu Thermal Power Plant with a capacity of 660 megawatts (Adana-Yumurtalik)
- Atlas Thermal Power Plant with a capacity of 1260 megawatts (Hatay-Iskenderun)
- Kojen Thermal Power Plant with a capacity of 15 megawatts (Kahramanmaras-Dulkadiroglu)

After the earthquake, the Afsin-Elbistan A and B thermal power plants were out of service, and the B plant was partially reopened after inspections. Some types of damage detected in industrial facilities throughout the region are shown in Figs. 27, 28, and 29).

Fig. 27 Structural damages (buckling in column reinforcements) in a new construction in a textile facility in Kahramanmaras

Fig. 28 Damages to non-structural elements (siding damage and machine-equipment damage) in a textile facility in Kahramanmaras

Iskenderun Port, one of the important ports in Turkey that provides transfer services to the Southern and Southeastern Anatolian Regions and Middle Eastern countries, had to suspend its operations due to a fire that broke out after the earthquake. The port management reported excessive settlements in some parts of the port structure and stated that the fire was caused by overturned containers. Additionally, damage was observed on the roads leading to the port. The fire at Iskenderun Port after the earthquake is shown in Fig. 30.

Fig. 29 A food facility in Gaziantep Nurdagi with damaged corn and wheat silos

Fig. 30 Fire in the Iskenderun Port after the earthquake (Anadolu Agency 2023a)

7 Evaluation of the infrastructure systems

Infrastructure systems, often referred to as lifeline systems, are critical for society as they provide essential services such as drinking water, wastewater management, natural gas, electricity, communication, and transportation. The functional continuity of these systems after an earthquake is crucial for both search and rescue operations and the well-being of citizens. For instance, damage to highways severely hindered search and rescue efforts and delayed aid delivery immediately following the earthquake. The earthquake caused serious damage to various infrastructure systems, prompting immediate efforts for damage assessment and restoration. The extensive coverage of these systems increased the number of damages and expanded the scope and scale of assessment and repair work. The time required to restore these systems varies, and the prevalence of collapsed and heavily damaged buildings has further complicated post-earthquake recovery efforts in residential areas.

7.1 Damages to water, wastewater, oil, natural gas, and electricity infrastructure systems

The infrastructure systems of a city, such as water supply and sewage, consist of various components, including pipes, pumping stations, and reservoirs. The performance of these systems relies on the seamless operation of all components to transport materials from the starting point to the desired endpoint. Any damage to these components can result in the failure of the entire system. This paper presents the damages encountered in different elements of the water supply and sewage systems during preliminary investigations.

Damage to buried pipeline systems caused by earthquakes can be categorized as temporary ground deformations (TGD) or permanent ground deformations (PGD) (Toprak and Taskin 2007). TGD refers to the dynamic response of the ground during the passage of earthquake waves, while PGD involves irreversible ground displacement after an earthquake. TGD can sometimes cause small amounts of permanent deformation, but these effects are generally superficial. In contrast, PGD is usually much larger and includes fault movements, landslides, displacement caused by liquefaction, and differential settlement in cohesionless soils (Toprak and Yoshizaki 2003; Toprak et al. 2024a)

Figure 31a shows the damage to water systems caused by faulting in the earthquake zone, where a drinking water pump station near the fault was seriously damaged, and the connection pipes were broken. Figure 31b shows a ductile pipeline damaged by faulting near Nurdagi. While the pipe body itself remained intact, separations occurred at the connection points. Figure 32 illustrates the damage caused by liquefaction at the stormwater and sewage elevation station on Ataturk Boulevard in Iskenderun. Figure 33

Fig. 31 Damages in water systems caused by fault movement

Fig. 32 Damages caused by liquefaction at the sewerage and storm water elevation station in Iskenderun

(a) Duzbag drinking water transmission line and tunnel

(b) Partial damage to the tunnel

(c) Damage to the pipe support

Fig. 33 Observations in Duzbag drinking water transmission line and tunnel presents observations from the Duzbag drinking water transmission line and tunnel. This system features a 2.6-m diameter steel conduit pipe running through a 3.5-km tunnel. Some damage occurred in the tunnel and pipe support system, as shown in Fig. 33. The tunnel, designed to protect the pipe and facilitate maintenance, functioned as intended, preventing damage to the pipe itself. The pipe responded to axial deformations with small movements at the connections. Following intensive repair and inspection efforts by GASKI and its support teams, water flow was restored to the city from the transmission line within three weeks after the earthquake.

Petroleum and Natural Gas Pipeline Operations in Turkey are managed by BOTAS, a State Economic Enterprise (KIT) established under Decree Law No. 233 and the decision of the Council of Ministers dated February 8, 1995. BOTAS is responsible for a wide range of services, including LNG/FSRU terminal operations, port services, project design related to petroleum and natural gas pipelines and compressor stations, engineering, land surveys, expropriation and construction works, natural gas and LNG trade, natural gas and LNG storage activities, and international natural gas and oil transportation projects. Following the earthquake, BOTAS announced on February 7, 2023, that there was damage in three regions where the natural gas main transmission line supplies gas to the provinces of Gaziantep, Kahramanmaras, and Hatay. Repair works continued at 18 locations under extremely difficult weather and terrain conditions (BOTAS 2023).

Gas distribution within residential areas is provided by private companies, requiring damage information to be obtained separately from each institution. For example, after GAZDAS provided natural gas to the city transmission network of BOTAS, it started supplying natural gas to hospitals and bakeries beginning February 13 (Anadolu Agency 2023b). Aksa Cukurova Natural Gas Distribution Co. announced on February 11 that, while network checks continued, they were able to supply natural gas to 99.4% of Adana, 91.4% of Osmaniye, and 100% of Mersin. In the Hatay region, one of the most affected by the earthquake, only 20.1% of subscribers had access to natural gas. Due to damages in BOTAS's Kahramanmaras-Gaziantep natural gas transmission line, gas could not be supplied to 137,422 subscribers in 34,381 buildings in the districts of Antakya, Arsuz, Iskenderun, Belen, Hassa, and Kirikhan in Hatay.

Electric power systems, crucial for modern infrastructure, were severely impacted by the February 2023 earthquakes. These systems, which supply energy to homes, healthcare, and emergency services, faced substantial challenges due to the seismic activity. Transmission and distribution lines, vital for delivering electricity over long distances, are particularly vulnerable during earthquakes. Supported by poles made of materials like wood, steel, concrete, or composites, these lines are designed to withstand environmental stresses under normal conditions. However, earthquakes can cause excessive swaying, structural stress, and potential failure of these poles. Ground shaking, liquefaction, landslides, rockfalls, and debris are major factors affecting the stability of transmission and distribution lines. Specific instances of damage included poles experiencing excessive swaying, structural stress, and potential failure due to ground shaking. Liquefaction caused the ground to lose its bearing capacity, leading to poles leaning, sinking, or collapsing. Landslides and rockfalls triggered by the earthquakes uprooted, broke, or buried poles under debris. Substations, critical for voltage conversion, power distribution, and grid connectivity, also suffered significant damage. Structural and equipment damage resulted in fire hazards and system interruptions. For instance, a column's foundation shifted, causing bending and separation from infill walls. Cracks and spalling were observed in the foundation, and a portion of the roof collapsed (e.g., Fig. 34). In

Fig. 34 Adana City Transformer Center TR184 Damage (Toprak et al. 2024b)

the village of Islahiye, Gaziantep, rockfalls caused extensive damage to the transformer center and electric poles, leading to the complete destruction of one pole.

An example of the impact on power generation facilities is the damage sustained by the Afsin-Elbistan B Thermal Power Plant, which has a capacity of 1,440 MW. This plant faced significant issues, including damage to the coal feeding systems, steam and gas-air lines, hot gas ducts, ash and coal filters, transformers, pumps, and valves. Additionally, extreme cold conditions led to freezing incidents in equipment and systems such as water and fire lines and heat exchangers. These damages highlight the vulnerabilities of electric power systems during seismic events. Ensuring the resilience of these systems involves improving the structural integrity of facilities, enhancing automated control systems, and developing comprehensive recovery and restoration plans to minimize the disruption of essential services during and after earthquakes.

7.2 Damages to highways, railways and airways

The fault lines intersect numerous points along the roads in the region. The existing highways and roads are crucial for providing access to the Mediterranean, Eastern Anatolia, and Southeastern Anatolia, making them vital as a major transit route. Significant horizontal and vertical displacements have occurred, particularly where the roads cross the fault lines, resulting in damage to the roads in Golbasi, Pazarcik, Nurdagi, and Reyhanli within the earthquake zone. Photographs between Figs. 35 36 37 38 and 39 illustrate the road and bridge damage in these areas. As shown in the figures, the roads have suffered horizontal and vertical offsets, especially at fault line intersections, leading to significant damage.

The region's railway network provides both domestic and international connections and, like the highways, intersects with faults at many points. The railway network

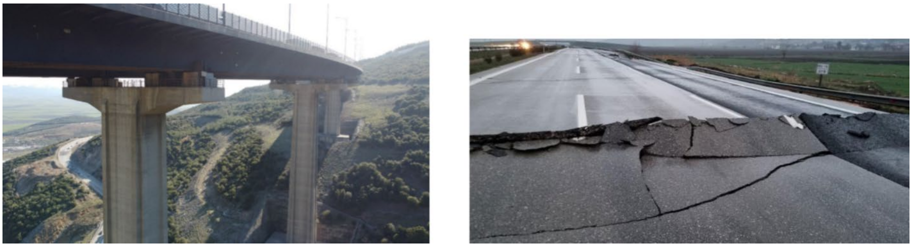

Fig. 35 Viaduct on TAG Highway: no damage to deck, columns, or supports; Tarsus-Adana-Gaziantep Highway: observed damage

Fig. 36 Damage observations on TAG highway viaduct

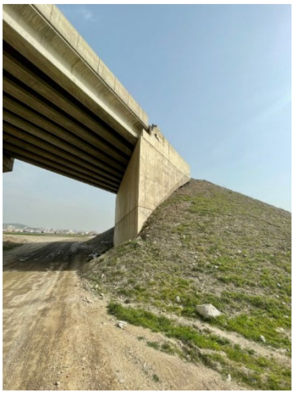

(a) Damage at the top edge of the abutment

(b) Nurdagi railway bridge: beam damages at the side abutment

Fig. 37 Nurdagi-Railroad bridge damages

(a) Damages on the road and pavement due to liquefaction in Iskenderun

b) Hatay-Reyhanli road damages

Fig. 38 Road damages in Hatay

Fig. 39 Damage observations at Pazarcik—Tevekkeli village road and fault intersection

includes bridges, tunnels, and other engineering structures. Damage observed along the railway line includes rail deformation due to ground movements, closure of tunnel entrances and exits caused by rock falls, and bridge damage. Examples of these and similar damages are shown in Fig. 40. Inspections at Kahramanmaras airport did not reveal any structural damage, but non-structural damage was identified (Fig. 41).

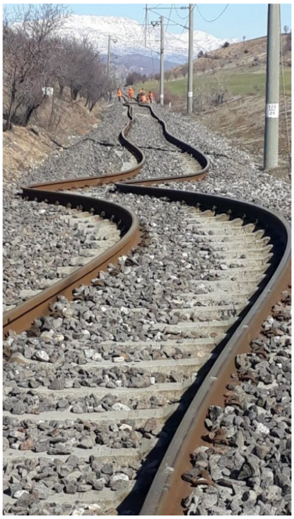

(a) Golbasi-Malatya railway line

b) Railway bridge - artwork and pier damage

(c) Closing of the tunnel entrance and damage to the tunnel structure due to rockfall and landslide at the railway line tunnel entrance

Fig. 40 Various damages at the railway, railway bridge and tunnel entrance/exit in the earthquake zone

8 Conclusions and recommendations

Following the February 6, 2023, earthquakes in the Kahramanmaras region of Turkey, the authors promptly responded to the disaster area. Their efforts included addressing urgent issues, such as verifying data in disaster crisis centers, evaluating the safety of critical structures, and planning immediate actions. They also collected crucial data for research and identified areas needing development. This paper details these observations and provides initial recommendations based on their evaluations and fieldwork.

Disaster management in Turkiye requires significant improvement, particularly for high-destruction events and adverse weather conditions. Detailed planning is urgently needed for the initial days following a disaster. The Kahramanmaras earthquakes revealed the poor condition of the existing building stock, with many buildings collapsing or suffering extensive damage, resulting in significant loss of life. It is crucial to

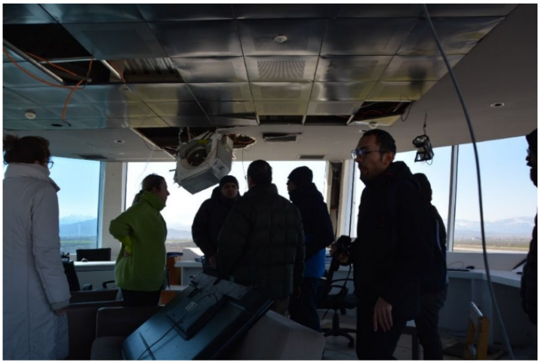

(a) Non-structural damage to the tower structure

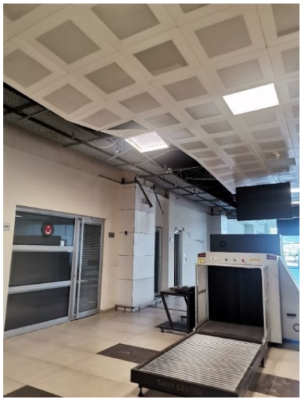

(b) Main building suspended ceiling damage

Fig. 41 Non-structural damages at Kahramanmaras Airport

urgently evaluate and improve the building inventory to make structures earthquake-resistant, possibly with government support for urban transformation.

Critical infrastructure and lifeline systems, including water supply, wastewater, oil, natural gas, and electricity networks, sustained serious damage due to fault line intersections and severe shaking. This included damage to roads, which hindered aid delivery, and to systems such as natural gas pipelines, disrupting essential services. Geohazards such as landslides, rockfalls, and slope failures further compromised infrastructure integrity. Soil problems like liquefaction were prominent in areas such as Iskenderun and Golbasi. Future studies will need to determine the primary causes of the damages. Reviewing these systems with more flexible structures and alternatives in mind is crucial for preparing for future earthquakes. Structural collapses and damaged buildings also affected telecommunications because base stations on the buildings were damaged. This disaster has highlighted the need to consider seismic effects in addition to electronic evaluations when determining base station locations and positions. Industrial facilities experienced various structural and non-structural damages, highlighting the need for a holistic approach to earthquake preparedness.

Key findings indicate that the earthquakes caused extensive surface ruptures and high ground accelerations, affecting structures in the area. Significant soil liquefaction was observed in areas like Golbasi and Iskenderun, contributing to structural damage. Buildings constructed before 2000, especially those with poor construction quality and non-compliance with regulations, suffered the most damage. Observations suggest that many collapses were related to construction quality, material deficiencies, and construction practices, in addition to the strong shaking caused by the earthquake. Further studies are needed to differentiate the exact causes of the damage before any changes to codes or regulations can be made. It is essential to thoroughly analyze the reasons for structural failures before making informed decisions about potential changes to seismic design codes and regulations.

Ongoing detailed geological and seismological studies are crucial for precise hazard mapping and risk assessment. The use of remote sensing technologies, like SAR interferometry, will enable real-time monitoring of ground deformations and damage, leading to more efficient disaster response. Enhancing public awareness and preparedness programs to educate communities about earthquake risks and safety measures is essential. Additionally, industrial facilities should implement contingency plans and structural reinforcements to minimize operational disruptions and economic losses during seismic events. The findings and recommendations from this study underscore the necessity for a multi-faceted approach to earthquake preparedness and resilience, integrating scientific research, engineering practices, and community engagement to mitigate the impacts of future seismic events.

Acknowledgements This study was supported by TUBITAK-1002C and Gebze Technical University. During the reconnaissance work, many individuals contributed to our team both institutionally and personally. We extend our gratitude to the authorities and staff of TOKI Sehit Jandarma Er Levent Kusoglu Primary School and Sehit Ali Riza Isbilir Anatolian High School for providing classrooms for accommodation. Special thanks to Dr. Assistant Professor Muammer Tun and his team responsible for the Elbistan Crisis Center; GASKI General Manager Huseyin Sonmezler, GASKI Treatment Facilities Manager Ahmet Ozturk, and all members of the field work team who provided support; PhD students Abdullah Erdogan and Berk Yagcioglu; officials of Kahramanmaras Dulkadiroglu Municipality; Ali Bayram Tunay from the Gaziantep Metropolitan Municipality Directorate of Urban Planning; our drivers, and all those who contributed but are not mentioned here. We thank them very much for their invaluable assistance during the extremely difficult times after the earthquakes.

Funding The authors declare that this study was supported by Gebze Technical University (GTU) and TUBITAK-1002C funding.

Declarations

Conflict of Interests The authors have no relevant financial or non-financial interests to disclose.

References

AFAD (2023) Disaster and Emergency Management Authority Presidential of Earthquake Department. http://tdvm.afad.gov.tr. Last accessed April 2023

Anadolu Agency (2023a) https://www.aa.com.tr/tr/gundem/iskenderun-limaninda-depremde-devrilen-onteynerlerde-cikan-yangina-ucakla-mudahale-/2810463

Anadolu Agency (2023b) https://www.aa.com.tr/tr/sirkethaberleri/enerji/zorlu-enerji-deprem-sonrasi-kontrollerin-ardindan-gaziantepte-dogal-gaz-arzina-baslayacak/678640

Akil B, Akpinar K, Uckardesler C, Araz H, Saglam M, Ecemis B, Uran SB (2008) Evaluation of settlement suitability of Golbasi (Adiyaman) Town, located on the East Anatolian Fault Zone. Geol Bull Turkey 51(1):43–57

Aktug B, Ozener H, Dogru A, Sabuncu A, Turgut B, Halicioglu K, Yilmaz O, Havazli E (2016) Slip rates and seismic potential on the East Anatolian Fault System using an improved GPS velocity field. J Geodyn 94–95:1–12

Allen CR (1969) Active faulting in northern Turkey. Divi Geol Sci, Calif Inst Technol, Contrib No 1577:32

Allen CR (1975) Geological criteria for evaluating seismicity. Geol Soc Am Bull 86(8):1041–1057

Ambraseys NN (1970) Some characteristic features of the Anatolian fault zone. Tectonophysics 9:143–165

Ambraseys NN (1989) Temporary seismic quiescence: SE Turkey. Geophys J Int 96(2):311–331

Ambraseys NN (2009) Earthquakes in the Mediterranean and Middle East In: a multidisciplinary study of seismicity up to 1900. Cambridge University Press

Arias A (1970) A measure of earthquake intensity. In: Hansen RJ (ed) Seismic design for nuclear power plants. MIT Press, Cambridge, Massachusetts, pp 438–483

Arpat E, Saroglu F (1972) The East Anatolian Fault System: thoughts on its development. Bull Miner Res Exploration (MTA) 78:33–39

Arpat E, Saroglu F (1975) Recent tectonic activities in Turkey. Bull Geol Soc Turkey 18:91–101

Arpat AE (1971) 22 Mayis, 1971 Bingol depremi on rapor. Institute of Mineral Research and Exploration Report No: 4697

Boore DM, Atkinson GM (2008) Ground-motion prediction equations for the average horizontal component of PGA, PGV, and 5%-damped PSA at spectral periods between 0.01 s and 10.0 s. Earthq Spectra 24:99–138. https://doi.org/10.1193/1.2830434

BOTAS (2023) https://www.botas.gov.tr/Icerik/buyuk-botas-ailesi-buyuk-turki/738

Cetin H, Guneyli H, Mayer L (2003) Paleoseismology of the Palu-Lake Hazar segment of the East Anatolian Fault Zone, Turkey. Tectonophysics 374:163–197. https://doi.org/10.1016/j.tecto.2003.08.003

Chiou BS-J, Youngs RR (2014) Update of the Chiou and Youngs NGA model for the average horizontal component of peak ground motion and response spectra. Earthq Spectra 30(3):1117–1153. https://doi.org/10.1193/072813EQS219M

Duman TY, Emre O (2013) The East Anatolian Fault: geometry, segmentation and jog characteristics. Geological Society. Special Publications, London, pp 495–529

Emre O, Duman T, Ozalp S, et al (2013) Active fault map of Turkey with an explanatory text 1:1.250.000 scale, Special Publication Series—30. General Directorate of Mineral Research and Exploration (MTA), Turkey

Farr TG, Rosen PA, Caro E et al (2007) The Shuttle radar topography mission. Rev Geophys 45:RG2004. https://doi.org/10.1029/2005RG000183

Garini E, Gazetas G (2023) Preliminary report on the M7.8 and M7.5 earthquakes of February 6, 2023 in Turkey-Syria. https://doi.org/10.17605/OSF.IO/V4MSW

Hajeb M, Karimzadeh S, Fallahi A (2020) Seismic damage assessment in Sarpole-Zahab town (Iran) using synthetic aperture radar (SAR) images and texture analysis. Nat Hazards 103:347–366

Heath DC, Wald DJ, Worden CB, Thompson EM, Smoczyk GM 2020 A global hybrid Vs30 map with a topographic-slope–based default and regional map insets USGS Earthquake Hazards Program, USGS Digital Object Identifier Catalog https://doi.org/10.5066/P96HFVXM

Italiano F, Sasmaz A, Yuce G, Okan OO (2013) Thermal fluids along the East Anatolian Fault Zone (EAFZ): Geochemical features and relationships with the tectonic setting. Chem Geol 339:103–114

Karimzadeh S, Samsonov S, Matsuoka M (2017) Block-based damage assessment of the 2012 Ahar-Varzaghan, Iran, earthquake through SAR remote sensing data. In Proceedings of the IEEE International Geoscience and Remote Sensing Symposium (IGARSS), FortWorth, TX, USA, 23–28 July 2017

Karimzadeh S, Matsuoka M (2018a) Building damage characterization for the 2016 Amatrice earthquake using ascending–descending COSMO-SkyMed data and topographic position index. IEEE J Sel Top Appl Earth Obs Remote Sens 11(8):2668–2682

Karimzadeh S, Matsuoka M (2018b) A weighted overlay method for liquefaction-related urban damage detection: a case study of the 6 September 2018 Hokkaido Eastern Iburi earthquake. Japan Geosci 8:487

Kocyigit A, Beyhan A (1998) A new intra-continental transcurrent structure: the central Anatolian fault zone, Turkey. Tectonophysics 284:317–336

KOERI (2023) Kandilli Observatory and Earthquake Research Institute. http://eida.koeri.boun.edu.tr. Last accessed April 2023

Kop A, Ezer M, Bodur MN, Darbas G, Inan S, Ergintav S, Seyis C, Yalcin C (2014) Geochemical monitoring along the Turkoglu (Kahramanmaras)-Golbasi (Adiyaman) segments of the east anatolian fault system. Arab J Sci Eng 39(7):5521–5536

Lermo J, Chávez-García FJ (1993) Site effect evaluation using spectral ratios with only one station. Bull Seismol Soc Am 83(5):1574–1594

McClusky S, Balassanian S, Barka A, Demir C, Ergintav S, Georgiev I, Gurkan O, Hamburger M, Hurst K, Kahle H et al (2000) Global Positioning System constraints on plate kinematics and dynamics in the eastern Mediterranean and Caucasus. J Geophys Res Solid Earth 105:5695–5719. https://doi.org/10.1029/1999JB900351

McKenzie D (1976) The East Anatolian Fault: a major structure in eastern Turkey. Earth Planet Sci Lett 29:189–193

Naji DM, Akin MK, Cabalar AF (2020) A comparative study on the V_{S30} and N_{30} based seismic site classification in Kahramanmaras, Turkey. Adv Civil Eng 2020:1–15

Nakamura Y (1989) A method for dynamic characteristics estimation of subsurface using microtremor on the ground surface. Q Rep Railw Tech Res Inst 30(1):25–33

USGS NEIC (2023) https://earthquake.usgs.gov/earthquakes/eventpage/us6000jllz/executive

Over S, Buyuksarac A, Bekta O, Filazi A (2011) Assessment of potential seismic hazard and site effect in Antakya (Hatay Province), SE Turkey. Environ Earth Sci 62:313–326

Reilinger R, McClusky S, Vernant P et al (2006) GPS constraints on continental deformation in the Africa-Arabia-Eurasia continental collision zone and implications for the dynamics of plate interactions. J Geophys Res Solid Earth 111:1–26. https://doi.org/10.1029/2005JB004051

Rotstein Y (1984) Counterclockwise rotation of the Anatolian block. Tectonophysics 108:71–91

Sandal EK, Karademir N (2013) The relationship between ground conditions and earthquake based on seismicity in Kahramanmaras. In 3rd International Geography Symposium-GEOMED 2013 Symposium Proceedings (pp. 474-488) (in Turkish with English abstract)
Sengor A, Gorur N, Saroglu F (1985) Strike-slip faulting and related basin formation in zones of tectonic escape: Turkey as a case study. In: Biddle K, Christie-Blick N (eds) Strike-slip deformation, basin formation and sedimentation. Society of Economic Paleontologists and Mineralogists, Tulsa, pp 227–264
TBDY (2018) Turkiye Bina Deprem Yonetmeligi, Afet ve Acil Durum Yonetimi Baskanligi, Resmi Gazete, Tarih: 18 Mart 2018, Sayi: 30364
Toktanis A, Over S (2021) Liquid pilot study in Konarli Neighborhood (Iskenderun). Geosound, 54(1):1-14 (in Turkish with English abstract)
Toprak S, Holzer TL (2003) Liquefaction potential index: field assessment. J Geotech Geoenviron 129(4):315–322. https://doi.org/10.1061/(ASCE)1090-0241(2003)129:4(315)
Toprak S, Nacaroglu E, Van Ballegooy S, Koc AC, Jacka M, Manav Y, Torvelainen E, O'Rourke TD (2019) Segmented pipeline damage predictions using liquefaction vulnerability parameters. Soil Dyn Earthq Eng 125:105758. https://doi.org/10.1016/j.soildyn.2019.105758
Toprak S, Taskin F (2007) Estimation of earthquake damage to buried pipelines caused by ground shaking. Nat Hazards 40:1–24. https://doi.org/10.1007/s11069-006-0002-1
Toprak S, Yoshizaki K (2003) Earthquake effects on buried pipelines. In Fifth National Earthquake Engineering Conference, 26–30 May, Istanbul (in Turkish with English abstract)
Toprak S, Wham BP, Nacaroglu E, Ceylan M, Dal O, Senturk AE (2024a) Impact of seismic geohazards on water supply systems and pipeline performance: insights from the 2023 Kahramanmaras Earthquakes. Eng Geol 340:107681. https://doi.org/10.1016/j.enggeo.2024.107681
Toprak S, Nacaroglu E, Wham B, Sakamoto M, Uckan E, Guldur Erkal B, Dal O, Ceylan M, Kaya ES, Bayraktar M, Senturk AE, Cappa R (2024b) Impacts and lessons from the February 2023 earthquakes on urban infrastructure systems. In: February 2023 Earthquakes Symposium from the Perspective of Civil/Earthquake Engineering. Chamber of Civil Engineers, Adana, Turkiye
Tugsal UM, Mutlu AK (2023) Development of open source software for use in earthquake engineering applications: DARLA (Version 1.0). DUJE 14(1):207–213. https://doi.org/10.24012/dumf.1247285
USGS (2023) https://www.usgs.gov/news/featured-story/m78-and-m75-kahramanmaras-earthquake-sequence-near-nurdagi-turkey-turkiye
Wald DJ, Quitoriano V, Heaton TH, Kanamori H (1999) Relationships between peak ground acceleration, peak ground velocity, and modifed Mercalli intensity in California. Earthq Spectra 15(3):557–564. https://doi.org/10.1193/1.1586058
Worden CB, Thompson EM, Hearne M, Wald DJ (2023) ShakeMap 4 Manual. https://usgs.github.io/shakemap/